Transport properties in anisotropic cross junctions by tight-binding calculations

Y. Takagaki and K. H. Ploog
Paul-Drude-Institut für Festkörperelektronik, Hausvogteiplatz 5-7, 10117 Berlin, Germany
(Received 30 March 2006; revised manuscript received 23 May 2006; published 18 August 2006)

Magnetotransport properties in anisotropic cross junctions are numerically investigated. We examine a system in which a uniaxial anisotropy of a two-dimensional electron gas leads to nonidentical transmission probabilities of an electron into the left- and right-hand-side leads. The Hall resistance in the absence of magnetic field is, as a direct consequence, nonzero. Its polarity changes periodically according to the location of the Fermi level with respect to the thresholds of one-dimensional subbands in the leads. The finite zero-field Hall resistance is not annihilated by potential disorder and is only weakly dependent on the number of occupied subbands. The anisotropy is manifested also at the transitions between quantum Hall plateaus.

DOI: 10.1103/PhysRevB.74.075325 PACS number(s): 73.23.−b, 72.15.Gd, 73.21.Hb, 73.43.Cd

I. INTRODUCTION

Using advanced molecular-beam-epitaxy technologies, two-dimensional electron gases (2DEG's) having extremely high mobilities can be realized in GaAs-(Al,Ga)As heterostructures. The improvement of the mobility is accomplished by eliminating residual impurities to ultralow levels. Consequently, ionized impurity scattering is less important for being the limiting factor of the low-temperature mobility. The mobility is instead significantly influenced by the properties of the heterointerface. For the most commonly used (001) surface orientation, the formation of elongated islands at the interface gives rise to a higher mobility along the $[\bar{1}10]$ direction than along the [110] direction.[1,2] In addition to this intrinsic anisotropy, the mobility can be forcefully made anisotropic by embedding, for instance, laterally modulated bunched steps[3] or self-assembled InAs dots.[4] The anisotropy may break the symmetry of transport properties in devices fabricated from such 2DEG's if the device geometry is defined in certain manners with respect to the anisotropy direction.

In this paper, we investigate the quantum transport properties in cross junctions delineated in an anisotropic 2DEG. In modeling the anisotropic system, we utilize a square tight-binding lattice with nonidentical nearest-neighbor hopping amplitudes in the two orthogonal directions. We establish a numerical procedure to calculate the quantum-mechanical transmission probabilities in such anisotropic devices. We reveal unique characteristics that are absent in isotropic counterparts.

II. NUMERICAL MODEL

A. Tight-binding model

We assume that a 2DEG has a uniaxial anisotropy. In order to take into account the anisotropy of the system, we employ a tight-binding square lattice having the nearest-neighbor hopping amplitudes t_1 and t_2 in the directions that are orthogonal to each other. (See the inset of Fig. 1.) A symmetrically shaped cross junction is defined by the square lattice as illustrated in Fig. 1. The cross junction is inclined with respect to the anisotropy direction. Apparently, the probabilities of an electron turning into the left-hand-side (LHS) and right-hand-side (RHS) leads are expected to be different. We calculate the transmission probabilities quantum-mechanically by extending the method that was originally developed by Ando[5] for an uninclined wire system.

B. Infinite wire

Let us first consider the propagation of an electron in an infinite wire, which is shown in Fig. 2, in the absence of magnetic field. As the number of the transverse lattice sites in the wire is not constant, the existing methods for numerical calculations are not immediately applicable. We describe below a numerical scheme for the inclined wire. Our method is not restricted to be for the 45° inclination but easily extendable for any inclination angles.

The wave equation for an electron having an energy E is given by

$$(E - H_{C,j})C_j + PD_{j-1} + QD_j = 0, \tag{1a}$$

$$(E - H_{D,j})D_j + Q^{\mathrm{T}}C_j + P^{\mathrm{T}}C_{j+1} = 0, \tag{1b}$$

where C_j and D_j are the wave amplitudes at the jth slices having N and $N+1$ transverse lattice sites, respectively. The

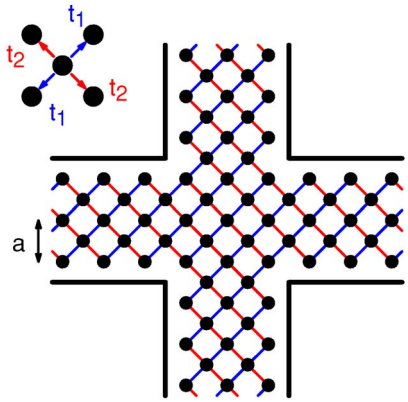

FIG. 1. (Color online) Tight-binding model for anisotropic cross junctions when the number of the transverse lattice sites is $N=2$. The thick solid lines indicate the boundary of the cross junction. The spacing between the nearest lattice sites of the square array is $a/\sqrt{2}$. The anisotropy is taken into account through the nearest-neighbor hopping amplitudes t_1 and t_2 as illustrated in the inset.

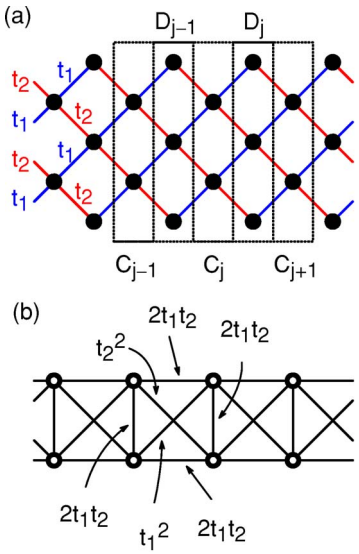

FIG. 2. (Color online) (a) Infinite wire simulated by using the anisotropic tight-binding model. The nearest-neighbor hopping amplitudes are t_1 and t_2. The wire is decomposed to slices containing transverse lattice sites as indicated by the dotted rectangles. C_j and D_j are the wave amplitudes at the jth slices having N and $N+1$ transverse lattice sites, respectively. (b) Tight-binding model equivalent to that in (a). The anisotropy of the system is expressed by the diagonal hoppings.

width of the wire is $W=(N+1)a$, where $a/\sqrt{2}$ is the spacing of the square lattice. H_C and H_D are diagonal matrices consisting of the on-site potentials. For the unrestricted hard-wall transverse confinement and in the absence of disorder, $H_C=H_D=0$. P and Q are $N\times(N+1)$ matrices given by

$$P=\begin{pmatrix} t_1 & t_2 & & 0 \\ & \ddots & \ddots & \\ 0 & & t_1 & t_2 \end{pmatrix}, \quad Q=\begin{pmatrix} t_2 & t_1 & & 0 \\ & \ddots & \ddots & \\ 0 & & t_2 & t_1 \end{pmatrix}. \tag{2}$$

Assuming $C_{j+1}=\lambda C_j$, the eigenmodes of Eq. (1) for a translationally invariant wire can be calculated numerically as solutions of[6]

$$\begin{bmatrix} H_3^{-1}H_1 & -H_3^{-1}H_2 \\ 1 & 0 \end{bmatrix}\begin{pmatrix} C_j \\ C_{j-1} \end{pmatrix}=\lambda\begin{pmatrix} C_j \\ C_{j-1} \end{pmatrix}, \tag{3}$$

where

$$H_1=E-H_C-P(E-H_D)^{-1}P^{\mathrm{T}}-Q(E-H_D)^{-1}Q^{\mathrm{T}}, \tag{4a}$$

$$H_2=P(E-H_D)^{-1}Q^{\mathrm{T}}, \tag{4b}$$

$$H_3=Q(E-H_D)^{-1}P^{\mathrm{T}}. \tag{4c}$$

In fact, the wave function of the nth mode when $H_C=H_D=0$ is given analytically as

$$u_n(j,l)\propto e^{ik_nja}e^{i\delta_nl}\sin\left(\frac{nl\pi}{N+1}\right). \tag{5}$$

The wave number k_n, which is related to λ as $\lambda_n=e^{ik_na}$, and the parameter δ_n are given as solutions of

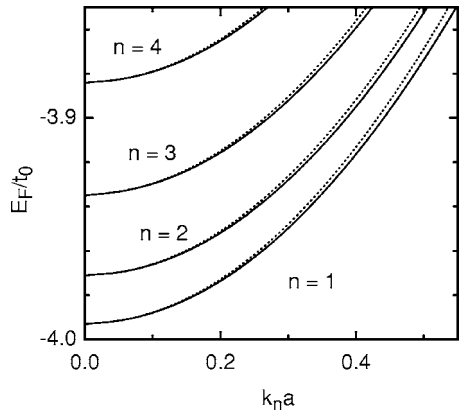

FIG. 3. Energy dispersion of the lowest four modes in a lead of width $N=25$. The nearest-neighbor hopping amplitudes are $t_1=1.2t_0$ and $t_2=0.8t_0$ for the solid curves and $t_1=t_2=t_0$ for the dotted curves.

$$\tilde{E}-\varepsilon_0-2t\cos\delta\cos\left(\frac{n\pi}{N+1}\right)-2t\cos(ka)$$
$$=2[\varepsilon_1\cos(ka+\delta)+\varepsilon_2\cos(ka-\delta)]\cos\left(\frac{n\pi}{N+1}\right), \tag{6a}$$

$$t\sin\delta+\varepsilon_1\sin(ka+\delta)-\varepsilon_2\sin(ka-\delta)=0. \tag{6b}$$

Here, $\tilde{E}=E^2$, $\varepsilon_1=t_1^2$, $\varepsilon_2=t_2^2$, $\varepsilon_0=2(\varepsilon_1+\varepsilon_2)$, and $t=2t_1t_2$. Note that the transverse wave function is no longer real for the anisotropic system, i.e., $\delta=0$ only if $t_1=t_2$.

It is worth noting that Eq. (1) can be reduced to

$$(\tilde{E}-H_0)C_j-\tilde{P}C_{j-1}-\tilde{P}^{\mathrm{T}}C_{j+1}=0, \tag{7}$$

where

$$H_0=\begin{pmatrix} \varepsilon_0 & t & & 0 \\ t & \varepsilon_0 & \ddots & \\ & \ddots & \ddots & t \\ 0 & & t & \varepsilon_0 \end{pmatrix}, \quad \tilde{P}=\begin{pmatrix} t & \varepsilon_2 & & 0 \\ \varepsilon_1 & t & \ddots & \\ & \ddots & \ddots & \varepsilon_2 \\ 0 & & \varepsilon_1 & t \end{pmatrix}. \tag{8}$$

The wave equation resembles that of ordinary uninclined wires. The lattice system in Fig. 2(a) is equivalent to that shown in Fig. 2(b). In the latter representation, the anisotropy is expressed in terms of the additional diagonal hoppings.

Figure 3 shows the energy dispersion of the lowest four modes when $N=25$. For the solid curves, the nearest-neighbor hopping amplitudes are assumed to be $t_1=1.2t_0$ and $t_2=0.8t_0$. For comparison, we include the dispersion for the isotropic case, $t_1=t_2=t_0$, by the dotted curves. The velocity v of the channels is given by $v=\hbar^{-1}\partial E/\partial k$. For the parameters in Fig. 3, the mode threshold energies are almost identical between the isotropic and anisotropic cases. However, the channel velocity is smaller in the anisotropic wire than in the isotropic wire. The velocity difference increases with increasing the energy.

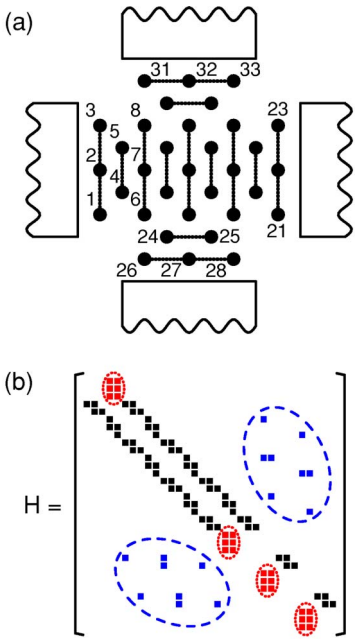

FIG. 4. (Color online) (a) Slice decomposition of the cross junction. Open boundaries, i.e., four semi-infinite leads, are attached to the finite-size cross junction. (b) Form of the truncated Hamiltonian matrix H corresponding to the lattice system shown in (a). The elements marked by the dotted ellipses contain information regarding the open boundaries. The coupling between the horizontal wire, the lattice sites 1–23 in (a), and the top and bottom lead, the lattice sites 24–33 in (a), is given by the elements marked by the dashed ellipses.

C. Cross junction

We now consider the cross junction in Fig. 1. As derived by Ando,[5] the transmission coefficient from mode n in lead α to mode m in lead β is related to the Green function $(\beta|G|\alpha)$ as

$$t_{\beta m,\alpha n} = \sqrt{v_m/v_n}[U_{+,\beta}^{-1}(\beta|G|\alpha)(F_{+,\alpha}^{-1} - F_{-,\alpha}^{-1})U_{+,\alpha}]_{mn}, \quad (9)$$

$$t_{\alpha m,\alpha n} = \sqrt{v_m/v_n}[U_{-,\alpha}^{-1}[(\alpha|G|\alpha)(F_{+,\alpha}^{-1} - F_{-,\alpha}^{-1}) - 1]U_{+,\alpha}]_{mn}, \quad (10)$$

where

$$F_{\pm} = U_{\pm}\Lambda_{\pm}U_{\pm}^{-1}. \quad (11)$$

The diagonal matrix Λ consists of λ_j and $U=(u_1,\ldots,u_N)$ contains the eigenfunctions u_j of the modes corresponding to λ_j. The plus and minus signs refer to the forward- and backward-propagating modes, respectively.

To calculate the Green function, we divide the cross junction into slices as illustrated in Fig. 4(a). The central portion of the cross junction is terminated by four uniform leads. This assumption allows us to truncate the open system to a system containing only a finite number of lattice sites. The "Hamiltonian" H is then described by a finite-size matrix, which has the form depicted in Fig. 4(b).[7] In this manner of site decomposition, the top and bottom leads are interpreted to be attached to the horizontal wire. The coupling between the horizontal wire and the two vertical leads is given by the matrix elements encircled by the dashed lines in Fig. 4(b). The elements encircled by the dotted lines provide information that semi-infinite leads are attached to the end slices of the finite cross junction. For instance, the wave equations at the two terminals of the horizontal wire read[5]

$$(E - H_{D,0})D_0 + [P^{\mathrm{T}} + Q^{\mathrm{T}}F_-^{-1}]C_1 = -Q^{\mathrm{T}}[F_+^{-1} - F_-^{-1}]C_{1,+}, \quad (12a)$$

$$(E - H_{D,M})D_M + [Q^{\mathrm{T}} + P^{\mathrm{T}}F_+]C_M = 0. \quad (12b)$$

The Green function is obtained as $G=(E-H)^{-1}$. The computation time to calculate the Green function can be greatly reduced if one employs the recursion technique to obtain only the relevant components of the Green function instead of inverting the whole matrix.[8]

We have so far assumed that the magnetic field is zero. In the presence of a magnetic field B, the hopping amplitudes acquire a phase factor $\exp[-i\hbar^{-1}\int e\mathbf{A}\cdot d\mathbf{l}]$. We have chosen to work using the gauge $\mathbf{A}=(-By/2, Bx/2, 0)$. In our numerical calculations, the magnetic field is gradually reduced to zero away from the cross junction in order to maintain translational invariance in the leads.[9]

III. RESULTS AND DISCUSSION

A. Transport properties at $B=0$

In Fig. 5, we show the energy dependence of the transmission probabilities in cross junctions when the size of the lattice system is $N=25$. Here, the cross junction is anisotropic in Fig. 5(a), $t_1=1.2t_0$ and $t_2=0.8t_0$, whereas it is isotropic in Fig. 5(b), $t_1=t_2=t_0$. The transport properties in the cross junctions are characterized by four transmission probabilities in the absence of magnetic field, which we define as $T_B=T_{11}$, $T_R=T_{21}$, $T_F=T_{31}$, and $T_L=T_{41}$, where $T_{\beta\alpha}=\Sigma_{m,n}|t_{\beta m,\alpha n}|^2$ is the transmission probability from lead α to lead β, see the inset in Fig. 5(b). (The probability conservation imposes a constraint among these transmission probabilities.) Note that T_R, for instance, is the probability of the transmission turning into the RHS lead for incidence from the horizontal leads but turning into the LHS lead for incidence from the vertical leads.

The population thresholds of one-dimensional (1D) modes in the leads are indicated by the bars in Fig. 5(a). Irrespective of the anisotropy, the forward transmission is enhanced and the transmission into the side leads is suppressed when E increases between adjacent thresholds. Such energy dependencies originate from the fact that the longitudinal momentum increases with E while the transverse momentum is kept constant due to its quantization for a given 1D channel.[10] This trend is evident in Fig. 6, in which the transmission probabilities are decomposed into each incident mode. At the opening of a new 1D channel, the backscattering is strongly enhanced and T_F exhibits a dip as the longitudinal momentum of the top-most subband is almost zero.

In the anisotropic system, T_R and T_L are no longer identical. For most of the energies, the LHS lead is preferred to the RHS lead when $t_1 > t_2$. However, T_R becomes larger than

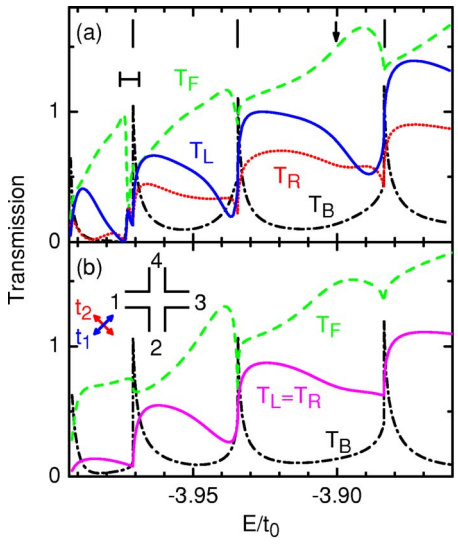

FIG. 5. (Color online) Energy dependence of the transmission probabilities in symmetrically shaped cross junctions in the absence of magnetic field for (a) $t_1=1.2t_0$ and $t_2=0.8t_0$ and (b) $t_1=t_2=t_0$. The probabilities of transmission into the left (T_L), front (T_F), right (T_R), and back (T_B) leads are shown by the solid, dashed, dotted, and dash-dotted curves, respectively. The number of transverse lattice sites is $N=25$. The bars in (a) indicate the population threshold of quasi-one-dimensional modes in the leads. The arrow indicates the equivalent position of the Fermi level in the calculations in Fig. 10. The horizontal line shows the energy range that is expanded in Fig. 8. The inset in (b) shows a schematic view of the cross junction.

T_L for a narrow energy interval below the threshold. The switching in the preference of the side leads is repeated regularly for each opening of a new channel. From the viewpoint of classical mechanics, forward-propagating electrons will be steered toward the LHS lead. However, the same consideration leads to the expectation that the RHS lead is favored when electrons are moving backward following a reflection from the cross junction. That T_R is generically larger than T_L before the opening of a new channel might imply that the

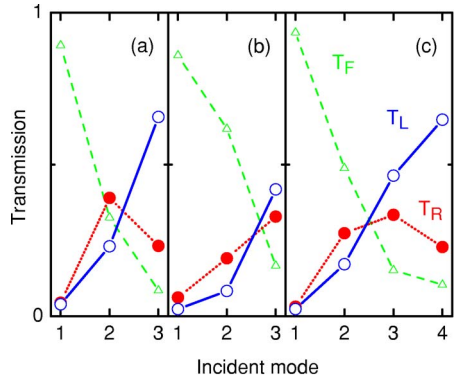

FIG. 6. (Color online) Transmission probabilities associated with individual incident modes in the absence of magnetic field, The Fermi energy is E/t_0=(a) −3.91, (b) −3.89, and (c) −3.86 with $t_1=1.2t_0$, $t_2=0.8t_0$, and $N=25$. The open circles, filled circles, and open triangles show the transmission probabilities into the left (T_L), right (T_R), and front (T_F) leads, respectively.

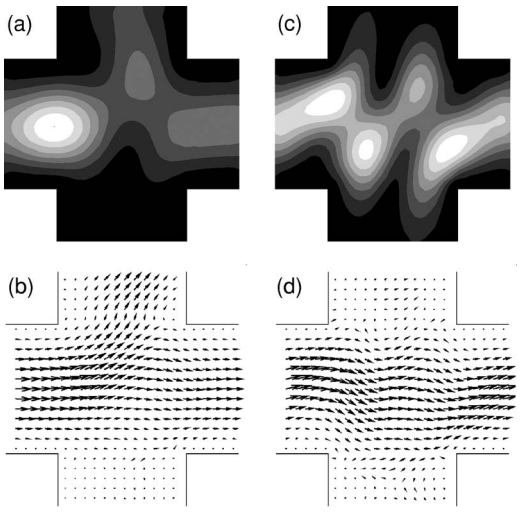

FIG. 7. Distributions of the probability density $|\Psi(x,y)|^2$, (a) and (c), and the equilibrium current $\mathbf{J}(x,y)$, (b) and (d), when an electron is incident from the left-hand-side lead. The Fermi energy is $E/t_0=-3.985$ in (a) and (b) and −3.975 in (c) and (d) with $t_1=1.2t_0$, $t_2=0.8t_0$, and $N=25$.

influence of the backscattering associated with the channel threshold is appreciable even for energies below the threshold in the anisotropic system. Nevertheless, the situation $T_R > T_L$ is realized around the energy at which T_F exhibits a peak. Therefore, we rather speculate that classical reflection from the cross-junction corner between the front and LHS leads gives rise to a dominance of backward propagation among those electrons that in the end enter the side leads, i.e., if the electrons do not enter the front lead. We point out that a reversal in the Hall coefficient is known to take place at weak magnetic fields in cross junctions having rounded corners. The incident electron beam is oriented toward the rounded corner by the magnetic field and then reflected into the "wrong" Hall probe.[11,12]

Interestingly, one finds in Fig. 6 that the transmission into the RHS lead is, in fact, generally larger than that into the LHS lead for the lower-lying modes. The reversal in the magnitudes of T_R and T_L occurs when T_L cannot be significantly larger than T_R for the higher-lying modes to overcome the trend of $T_R > T_L$ for the lower-lying modes. In order to further examine the origin of the switching behavior, we plot in Fig. 7 the distributions of the probability density $|\Psi(x,y)|^2$ and the equilibrium current $\mathbf{J}(x,y)$.[8] Figures 7(a) and 7(b) are for the case of $T_L > T_R$ ($E=-3.985t_0$), whereas Figs. 7(c) and 7(d) are for the case of $T_L < T_R$ ($E=-3.975t_0$). The peak in $|\Psi(x,y)|^2$ for $E=-3.985t_0$ at the junction between the LHS lead and the cross center is due to the quantum-mechanical backscattering into the incident lead by the junction interface. The weak peak near the upper-right corner of the cross center implies a reflection from this corner. (The reflection is purely quantum-mechanical in contrast to the classical reflection from a rounded corner.) Apart from these features, the relatively smooth and uniform distributions of $|\Psi(x,y)|^2$ and $\mathbf{J}(x,y)$ indicate that the situation $T_L > T_R$ is the intrinsic nature of the anisotropic system, plausibly realized as the backward-propagating wave components within the cross

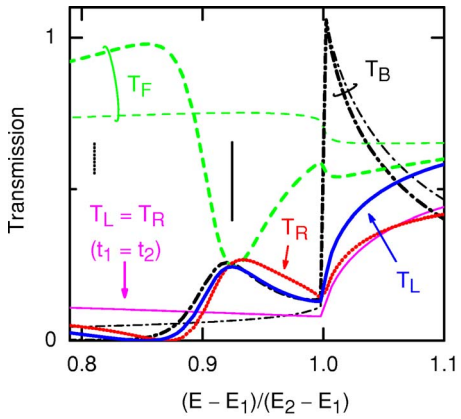

FIG. 8. (Color online) Transmission resonance in the anisotropic cross junction. The solid, dashed, dotted, and dash-dotted curves show the transmission probabilities into the left (T_L), front (T_F), right (T_R), and back (T_B) leads, respectively. The four transmission probabilities become almost identical at the transmission resonance indicated by the solid bar. The energy E is normalized using the threshold energies E_1 and E_2 of the bottom two 1D channels. The nearest-neighbor hopping amplitudes are $t_1=1.2t_0$ and $t_2=0.8t_0$ for the thick curves and $t_1=t_2=t_0$ for the thin curves with $N=25$. The transmission resonance is absent for the isotropic case. The dotted bar shows the position of the energy for Fig. 7(c) and 7(d).

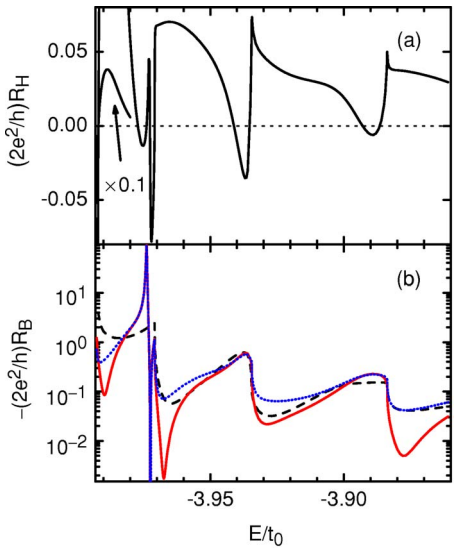

FIG. 9. (Color online) (a) Hall resistance R_H and (b) bend resistance R_B at zero magnetic field calculated using the transmission probabilities plotted in Fig. 5. The solid and dotted curves in (b), respectively, show $R_{B,1}=R_{43,12}$ and $R_{B,2}=R_{23,14}$ when $t_1=1.2t_0$ and $t_2=0.8t_0$. The dashed curve shows R_B when $t_1=t_2=t_0$.

center are small. For the extraordinary situation $T_R>T_L$, on the contrary, $|\Psi(x,y)|^2$ exhibits a multiple-nodes standing-wave-like pattern and meandering is observed in $\mathbf{J}(x,y)$, indicating strong reflections, and thus significant backward propagation, within the cross center.[13]

For the anisotropic cross junction, a transmission resonance takes place at an energy slightly below the population threshold of the second channel. We show the transmission probabilities in the vicinity of this transmission resonance with an expanded energy scale in Fig. 8. [The energy range is indicated by the horizontal line in Fig. 5(a).] The energy E is normalized using the threshold energies E_1 and E_2, respectively, of the lowest and the second 1D subbands for two sets of the hopping amplitudes. The resonance is associated with two bound states that exist in a cross junction due to the weak quantum-mechanical confinement at the crossing of two orthogonal wires in comparison to that in an individual wire. In a symmetric and isotropic cross junction,[14] a bound state having even parity of the wave function exists at an energy slightly below the population threshold of the lowest mode in the leads. As this bound state is energetically inaccessible by the state in the leads, it is irrelevant for the transport properties, unless inelastic scattering into and out of the bound state is permitted. The other bound state is located at an energy slightly below the population threshold of the second mode in the leads. An electron can, in principle, be injected into this bound state from the bottom channel in the leads. However, as the bound state possesses odd parity, parity mismatch forbids the coupling between this bound state and the lead state in the symmetric system. The even-odd decoupling ceases if the symmetry of the system is broken, including when the system is anisotropic. [Microscopically, the coupling between the lead state and the quasibound state is due to the phase δ in Eq. (5).] The resultant coupling gives rise to the transmission resonance, indicated by the bar, in Fig. 8.[15]

In Fig. 9, we show the Hall resistance $R_H=R_{42,13}$ and the bend resistance R_B calculated using the transmission probabilities plotted in Fig. 5. Here, $R_{ij,kl}=(V_i-V_j)/I_{kl}$ indicates that the four-terminal resistance is defined using the voltage difference between leads i and j when a current flows from lead k to lead l.[16] Depending on the lead configuration with respect to the anisotropy direction, R_B can take two different values as

$$R_{B,1}=R_{43,12}=\frac{h}{2e^2}\frac{T_L-T_F}{2(T_R+T_L)(T_F+T_R)}, \tag{13a}$$

$$R_{B,2}=R_{23,14}=\frac{h}{2e^2}\frac{T_R-T_F}{2(T_R+T_L)(T_F+T_L)}. \tag{13b}$$

On the contrary, Onsager symmetry shows that the anisotropy results only in the reversal of the magnetic field direction for

$$R_H=\frac{h}{2e^2}\frac{T_L-T_R}{2(T_F+T_L)(T_F+T_R)}, \tag{14}$$

i.e., the reversal of the sign at $B=0$.

As $T_R\neq T_L$, the Hall voltage is nonzero even for $B=0$. Its sign changes regularly as a consequence of the size reversal between T_R and T_L. At the transmission resonance, the transmission probabilities become nearly identical. Consequently, R_H and R_B change drastically and R_B can be even positive at $E\approx-3.972t_0$. The negative resistance in R_B decays rapidly with increasing the Fermi energy. The magnitude is roughly inversely proportional to the number of modes in the leads

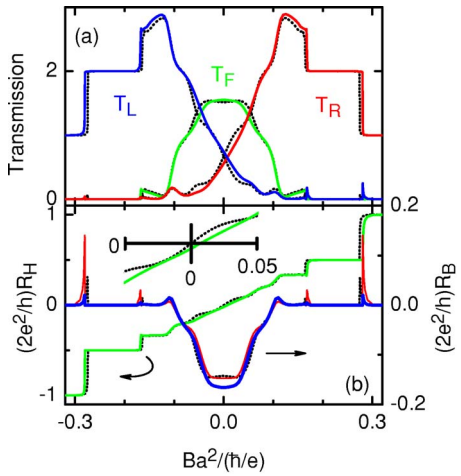

FIG. 10. (Color online) (a) Transmission probabilities and (b) Hall resistance R_H and bend resistance R_B in the presence of a magnetic field B. The solid and dotted curves correspond to $t_1=1.2t_0$ and $t_2=0.8t_0$ and $t_1=t_2=t_0$, respectively. Numerical parameters are $N=12$ and $E=-3.6t_0$, for which the equivalent Fermi level is located as shown by the arrow in Fig. 5(a). $R_{B,1}=R_{43,12}$ and $R_{B,2}=R_{23,14}$ are shown in (b) by the thick and thin solid curves, respectively. The inset in (b) shows R_H around zero magnetic field with expanded scales.

below the Fermi level. In contrast, the finite zero-field Hall voltage depends only weakly on the number of occupied modes, except for the single-mode regime.

B. Transport properties at $B \neq 0$

Figure 10(a) shows the magnetic-field dependence of the transmission probabilities. We have assumed $N=12$ and $E=-3.6t_0$. These parameters correspond to the Fermi level indicated by the arrow in Fig. 5(a). That is, three 1D subbands are occupied below the Fermi level at $B=0$. In order to simulate a general circumstance, the Fermi level has been chosen here to be in the regime of $T_L > T_R$. The hopping amplitudes are chosen as before to be $t_1/t_2=1.2/0.8$ and 1 for the solid and dotted curves, respectively.

The transmission is not identical when an electron is injected from the horizontal leads or from the vertical leads. The transport properties are thus governed, in principle, by eight transmission probabilities in the presence of a magnetic field. Consequently, Eqs. (13) and (14) are no longer valid when $B \neq 0$. However, there exist symmetry relationships, for example, $T_R(B)=T_{21}(B)=T_{12}(-B)=\tilde{T}_L(-B)$ and $T_L(B)=T_{41}(B)=T_{14}(-B)=\tilde{T}_R(-B)$, where the tilde indicates the case that an electron is injected from a vertical lead instead of a horizontal lead. The forward transmission probability is a symmetric function of magnetic field, and so T_F is independent of the lead from which an electron is injected. Therefore, the number of independent transmission probabilities is actually the same irrespective of the presence of the magnetic field. We, therefore, show in Fig. 10(a) only the transmission probabilities when an electron is injected from a horizontal lead.

The corresponding R_H and R_B are plotted in Fig. 10(b). In the inset of Fig. 10(b), we show R_H near zero magnetic field with expanded scales. Apart from an offset, i.e., the nonzero R_H at $B=0$, R_H varies nearly linearly with B even in the anisotropic system.

C. Effects of disorder

We have so far demonstrated that R_H in the anisotropic cross junction is finite at zero magnetic field. In experimental situations, there are a number of effects that may suppress the nonzero R_H; the occupation of multiple 1D modes, the finite temperature, and a disorder. The first two effects are indicated to be insignificant. We have already shown that the dependence of the nonzero R_H on the number of 1D modes is much weaker than that for the negative bend resistance phenomenon. Although the sign of the nonzero R_H changes with E, thermal averaging is unlikely to diminish the nonzero value as the opposite sign in R_H occurs only in narrow energy ranges. In this subsection, we consider the third issue, i.e., the influence of disorder. It should be noted that the shape of the corners of the cross junction is known to affect R_H at weak magnetic fields.[11] The geometry effect is insignificant when the magnetic field is exactly zero in an isotropic system. We ignore the geometry effect as it is beyond the scope of the present study.

We introduce a short-range disorder inside the square region at the center of the cross junction of width W. Within the disordered region, the site potential is modified randomly assuming a uniform distribution of correction potentials between $-d/2$ and $d/2$. We have averaged the transmission probabilities over typically a few hundred disorder realizations.

In Fig. 11(a), we compare the transmission probabilities in the anisotropic system between fully ballistic and moderately disordered transport regimes. The disorder reduces T_F at $B=0$ considerably while the transmission into the side leads is barely changed. The difference between T_L and T_R at $B=0$ is almost independent on the disorder, and so R_H around $B=0$ remains nearly the same as shown in Fig. 11(b).

The transport in the cross junction is still in the quasiballistic regime in Fig. 11, as evidenced by the negative value of R_B at $B=0$ shown in Fig. 11(c). When the disorder is further strengthened so as to reduce the mean free path of electrons to be shorter than the size W of the cross junction, the nonzero R_H may vanish as $T_L \approx T_R \approx T_F$ is anticipated.[17] Specifically, as electrons will diffuse in the cross junction in arbitrary directions with equal probabilities, the anisotropy contribution to T_L and T_R may average out. We have, therefore, examined in Fig. 12 the variation of the transmission at zero magnetic field between the ballistic and diffusive transport regimes. Independent of the disorder strength, the difference between T_L and T_R is almost constant when $T_L > T_R$. In contrast, the situation $T_L < T_R$ that occurs over narrow energy ranges below subband thresholds is turned around into the ordinary case of $T_L > T_R$. Remarkably, the difference $T_L - T_R$ in the diffusive transport regime is found to be independent of the Fermi energy and remains to be finite. The reason for the energy independence is not clear at present.

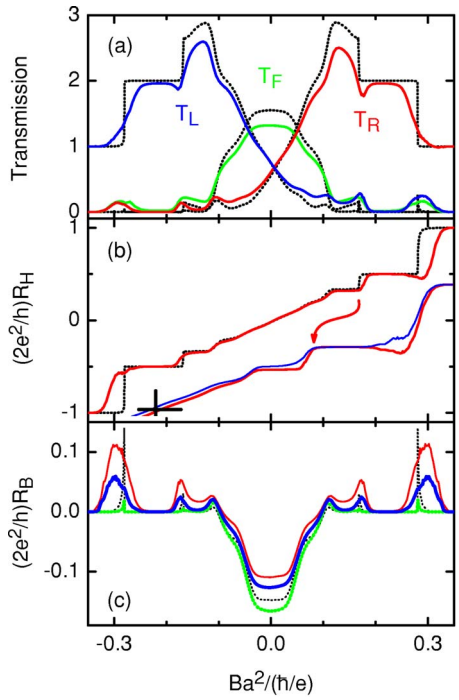

FIG. 11. (Color online) (a) Dependence on magnetic field B of the transmission probabilities into the left (T_L), front (T_F), and right (T_R) leads averaged over short-range disorder potentials. Hall resistance R_H and bend resistance R_B calculated using the disorder-averaged transmission probabilities are shown in (b) and (c), respectively. The strength of the disorder is $d/t_0=0.7$ and 0 for the solid and dotted curves, respectively. The inset in (b) shows $R_H(B)$ in the positive magnetic-field direction with expanded scales (thick curve) together with $-R_H(-B)$ (thin curve). The thick and thin curves in (c) correspond to $R_{B,1}=R_{43,12}$ and $R_{B,2}=R_{23,14}$, respectively.

However, we would like to point out possible explanations. As one finds in Figs. 7(a) and 7(b), the LHS lead will be preferred if electrons directly enter one of the side leads. Ballistic reflections from the cross boundary are essential, as shown in Figs. 7(c) and 7(d), if the situation $T_L<T_R$ occurs. As the disorder was assumed in our simulation only in the cross center, the former contribution may remain effective while the latter contribution is vanished by the disorder scattering. Nevertheless, the astonishing degree of the energy independence in the disordered regime suggests the existence of a fundamental principle beyond our qualitative explanation. For instance, the short-range disorder potential might give rise to a certain kind of energy averaging, leading to the transmission feature being independent of the incident energy.

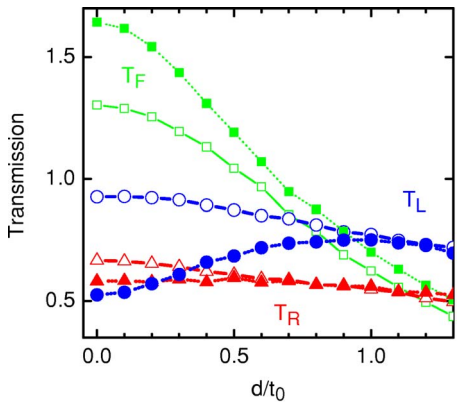

FIG. 12. (Color online) Dependence of the transmission probabilities on the disorder strength d when $t_1=1.2t_0$, $t_2=0.8t_0$, and $N=25$. The circles, triangles, and squares show the transmission probabilities into the left (T_L), right (T_R), and front (T_F) leads, respectively. The Fermi energy is $E/t_0=-3.91$ and -3.89 for the open and filled symbols, respectively.

Another contribution of disorder to the transport properties is to smear the transition between quantum Hall plateaus in high magnetic fields. In a ballistic system, the transition occurs abruptly at the magnetic depopulation thresholds of the 1D subbands. On the contrary, the transition is gradual when disorder is introduced. It is worth noting that localized edge states are formed around potential peaks and valleys in very high magnetic fields. The transmission curves for an individual realization of the potential disorder reveals sharp transmission resonances through these localized states at the transition between quantum Hall plateaus (not shown). These resonances are responsible for the residual fluctuations in the curves in Fig. 11 around $B=\pm 0.3\hbar/(ea^2)$ despite averaging over, at least, 500 ensembles. In the inset of Fig. 11(b), we compare the disorder-averaged R_H in the anisotropic system (thick solid curve) with $-R_H(-B)$ (thin solid curve). The anisotropy is found to give rise to a significant difference in the magnitude of R_H at the transition regions. The effect of the anisotropy is seen here to be shifting the trace of R_H horizontally. This means that the anisotropy acts as an effective magnetic-field bias.

In addition to the anisotropy effects, we point out a notable feature in Fig. 11(b); R_H decreases at $B\approx 0.29\hbar/(ea^2)$ with increasing B before eventually evolving into the next quantum Hall plateau. Such overshootlike behavior is sometimes observed experimentally, especially in low-mobility systems. Our numerical result shows that the anomalous feature can originate from transmission resonances through disorder-induced localized edge states.

IV. SUMMARY AND REMARKS

We have investigated the transport properties of an electron in symmetrically shaped cross junctions defined in an anisotropic system. Quantum-mechanical transmission probabilities have been calculated using a tight-binding model. The anisotropy has been found to break the symmetry of the electronic state and the transport symmetry, giving rise to a transmission resonance through a quasibound state in the cross junction and a finite Hall resistance despite the absence of magnetic field, respectively. We have shown that the finite Hall resistance is robust against disorder and its magnitude depends, except in the single-mode regime, only weakly on the number of occupied subbands in the leads. While the nonzero Hall resistance is, in principle, of classical origin, periodic switching in the polarity of the finite Hall resistance associated with subband thresholds takes place in the quantum-mechanical situation. The Hall resistance is found

to develop a significant nonantisymmetry also at the transitions between quantum Hall plateaus.

We have assumed an intrinsic anisotropy in our model. In the experimental situation using 2DEG's in GaAs-(Al,Ga)As heterostructures, the anisotropy will arise from the elongated features at the heterointerface or intentionally embedded nanostructures. The electron transport in such circumstances is anticipated to become isotropic in the fully ballistic regime, i.e., if the size of the cross junction is reduced to be even smaller than the length scales of the objects that give rise to the anisotropy. Our theoretical predictions are, therefore, applicable when the cross junctions are much larger than the elongated objects but smaller than (comparable with) the elastic mean-free path of electrons, plausibly imposed by the residual impurity scattering, for the ballistic (quasiballistic) transport regime of our simulations.

Throughout our study, we have ignored the influence of rounded corners. In experimental cross junctions consisting of quantum wires, i.e., when the wire width is comparable to the Fermi wavelength of an electron, the dominance of geometry effects is fairly inevitable as unintentional rounding is present due to the surface depletion, which is typically on the order of submicrometers. Large cross junctions defined in extremely-high-mobility 2DEG's are hence ideal to examine the predicted features around zero magnetic field in order to realize angular corners. Our prediction of the nonidentical transition behavior between the quantum Hall plateaus upon reversal of the direction of magnetic field is, in contrast, expected to be valid regardless of the junction geometry. The electron transport in high magnetic fields takes place in the form of edge states. The edge states travel along the channel boundary at a distance of the cyclotron radius irrespective of its shape.

ACKNOWLEDGMENT

The authors would like to thank K.-J. Friedland for turning their attention to the transport symmetry in an anisotropic system.

[1] Y. Tokura, T. Saku, and Y. Horikoshi, Phys. Rev. B **53**, R10528 (1996); Y. Tokura, T. Saku, S. Tarucha, and Y. Horikoshi, *ibid.* **46**, 15558 (1992).

[2] Y. Markus, U. Meirav, H. Shtrikman, and B. Laikhtman, Semicond. Sci. Technol. **9**, 1297 (1994).

[3] H.-P. Schönherr, J. Fricke, Z. Niu, K.-J. Friedland, R. Nötzel, and K. H. Ploog, Appl. Phys. Lett. **72**, 566 (1998).

[4] G.-H. Kim, D. A. Ritchie, C.-T. Liang, G. D. Lian, J. Yuan, M. Pepper, and L. M. Brown, Appl. Phys. Lett. **78**, 3896 (2001).

[5] T. Ando, Phys. Rev. B **44**, 8017 (1991).

[6] The number of independent modes in the wire is N. One can construct an equation for D_j, which is similar to Eq. (3). However, the equation does not have solutions. This is consistent with the fact that Eq. (7) is expressed in terms of C_j.

[7] M. J. McLennan, Y. Lee, and S. Datta, Phys. Rev. B **43**, 13846 (1991).

[8] H. U. Baranger, D. P. DiVincenzo, R. A. Jalabert, and A. D. Stone, Phys. Rev. B **44**, 10637 (1991).

[9] Y. Takagaki, Y. Hirayama, T. Saku, and S. Tarucha, Phys. Rev. B **53**, 10060 (1996).

[10] H. U. Baranger, Phys. Rev. B **42**, 11479 (1990).

[11] C. J. B. Ford, S. Washburn, M. Büttiker, C. M. Knoedler, and J. M. Hong, Phys. Rev. Lett. **62**, 2724 (1989).

[12] C. W. J. Beenakker and H. van Houten, Phys. Rev. Lett. **63**, 1857 (1989).

[13] We emphasize that the standing-wave-like pattern in Fig. 7(c) is not due to a transmission resonance. See the dotted bar in Fig. 8 that indicates the energy $E=-3.975t_0$ for Figs. 7(c) and 7(d).

[14] R. L. Schult, D. G. Ravenhall, and H. W. Wyld, Phys. Rev. B **39**, 5476 (1989); R. L. Schult, H. W. Wyld, and D. G. Ravenhall, *ibid.* **41**, 12760 (1990).

[15] If the cross center is enlarged, for instance, by rounded corners, the confinement modes are lowered in energy in the cross region and result in a number of quasibound states. The transmission properties are overwhelmingly dominated by the transmission resonances irrespective of the anisotropy. See Y. Takagaki and D. K. Ferry, Phys. Rev. B **44**, 8399 (1991).

[16] M. Büttiker, Phys. Rev. Lett. **57**, 1761 (1986).

[17] Y. Takagaki, K. Gamo, S. Namba, S. Ishida, S. Takaoka, K. Murase, K. Ishibashi, and Y. Aoyagi, Solid State Commun. **68**, 1051 (1988).